Hindawi Publishing Corporation
Journal of Nanomaterials
Volume 2015, Article ID 401656, 8 pages
http://dx.doi.org/10.1155/2015/401656

Research Article

EG-Assisted Synthesis and Electrochemical Performance of Ultrathin Carbon-Coated $LiMnPO_4$ Nanoplates as Cathodes in Lithium Ion Batteries

Liwei Su,[1] Yali Sha,[1] Jingkang Jiang,[1] Lianbang Wang,[1] and Yuanhao Wang[2]

[1]*State Key Laboratory Breeding Base of Green Chemistry-Synthesis Technology, College of Chemical Engineering, Zhejiang University of Technology, Hangzhou 310014, China*
[2]*Faculty of Science and Technology, Technological and Higher Education Institute of Hong Kong, New Territories, Hong Kong*

Correspondence should be addressed to Lianbang Wang; wanglb99@zjut.edu.cn and Yuanhao Wang; yuanhaowang@yahoo.com

Received 2 March 2015; Accepted 2 April 2015

Academic Editor: Lei Shao

Ultrathin carbon-coated $LiMnPO_4$ (ULMP/C) nanoplates were prepared through an ethylene glycol- (EG-) assisted pyrolysis method. Different from most of $LiMnPO_4$/C works, the obtained ULMP/C possessed relatively small particle size (less than 50 nm in thickness) and preferable carbon coating (~1 nm in thickness, 2 wt.%). As a reference, $LiMnPO_4$/C (LMP/C) composites were also fabricated via the traditional hydrothermal method. X-ray diffraction (XRD), scanning electron microscopy (SEM), transmission electron microscopy (TEM), energy dispersive X-ray spectroscopy (EDS), thermogravimetric analysis (TG), galvanostatic charge-discharge, and cyclic voltammetry (CV) were performed to characterize the crystalline phase, morphology, structure, carbon content, and electrochemical behaviors of samples. The electrochemical performance of bare and carbon-coated $LiMnPO_4$ was evaluated as cathodes in lithium ion batteries. As a result, the obtained ULMP/C nanoplates demonstrated much higher reversible capacities (110.9 mAh g^{-1} after 50 cycles at 0.1 C) and rate performances than pure LMP and LMP/C composites. This facile and efficient EG-assisted pyrolysis method can enlighten us on exploiting advanced routes to modify active materials with ultrathin and homogeneous carbon layers.

1. Introduction

Lithium ion batteries (LIBs), firstly commercially manufactured by Sony Company in 1991, are believed to be one of the most promising devices in terms of high energy/power density, environmental friendliness, and good safety and as a result they have been attracting intensive attentions in the ever-increasing requirements of portable devices and electric vehicles [1–5]. Ideal active materials for lithium storage should possess a host structure to store a significant amount of Li (i), be chemically and physically stable in the operating potential window (ii), have good electronic and ionic conductivity (iii), and be inexpensive and nontoxic (iv) [6]. Compared with the extensively studied and commercialized $LiFePO_4$, $LiMnPO_4$ possesses the similar theoretical capacity (~170 mAh g^{-1}), low cost, and the same olivine structure with the rigid phosphate network and desirable electron/Li^+ transfer paths [7]. More importantly, $LiMnPO_4$ delivers a much higher redox voltage (4.1 V versus Li/Li^+) than that (3.4 V versus Li/Li^+) of $LiFePO_4$, indicating a preferable power density and larger application potentials [8]. However, the intrinsically poor electronic conductivity ($<10^{-10}$ S cm^{-1}) and Li^+ ion diffusion ($<10^{-7}$ cm^2 s^{-1}) seriously restrict the lithiation/delithiation capability, especially the rate performances of $LiMnPO_4$ [9]. Moreover, the relative large volume variation (~10%) during cycling and the gradual dissolution/loss of Mn^{2+} ions into the electrolyte make it difficult for practical applications [10].

To overcome these shortcomings, great efforts have been made and they mainly focused on three strategies: (i) adjusting particle size and morphology to reduce the transport path length of electrons and Li^+ ions [11–13], (ii) doping with divalent or high valence cations to enhance conductivity [14–16], and (iii) surface modification with highly conductive

inorganic compounds and conductive polymers [17–20]. Rangappa et al. reported a supercritical ethanol process to prepare $LiMnPO_4$ nanorods with different particle sizes (20–80 nm), and the particles with smaller sizes exhibited higher reversible capacities [21]. Various methods, such as sol-gel method, spray pyrolysis, solid state reaction, hydrothermal/solvothermal synthesis, and polyol reflux synthesis, have been adopted to synthesize $LiMnPO_4$ nanomaterials with different morphologies [22–27]. Among them, hydrothermal/solvothermal methods have been widely used due to the facile operation, mild condition, and easy to obtain uniform particles. Nevertheless, recent researches indicated that only reducing the primary particles to hundreds or even tens of nanometers was unable to compensate the sluggish kinetics and acquire desired rate capability [28, 29]. As a result, combining $LiMnPO_4$ with conductive materials such as the stable and high-conductivity carbon layers was an effective compensation. With high-energy ball milling of $LiMnPO_4$ particles and conductive carbon materials [30–33], the carbon layer on the surface of $LiMnPO_4$ particles was too massy and could be easily stripped owing to strong friction during the stirring procedure. Hydrothermal synthesis was also an effective way to fabricate carbon-coated active materials especially metal oxide anodes [34]. However, carbon sources in the hydrothermal conditions were difficult to absorb on the surface of $LiMnPO_4$ without any modification. Moreover, this route generally led to a high carbon content (>10 wt.%), accompanied with the formation of carbon microspheres. Besides, the hydrothermal treatment was limited for large production to some extent. Therefore, it is significant to develop an efficient and low-cost strategy to encapsulate $LiMnPO_4$ particles with an ultrathin and homogeneous carbon layer.

In this work, ultrathin carbon-coated $LiMnPO_4$ (ULMP/C) nanoplates were prepared through an ethylene glycol- (EG-) assisted pyrolysis method. Different from most of $LiMnPO_4$/C works, the obtained ULMP/C possessed relatively small particle size (less than 50 nm in thickness) and preferable carbon coating (~1 nm in thickness, 2 wt.%). The ULMP/C nanoplates demonstrated considerable capacities (110.9 mAh g^{-1} after 50 cycles at 0.1 C) and rate performances. The EG-assisted pyrolysis method was facile, efficient, and suitable for large production and might enlighten us on exploiting advanced routes to modify active materials with ultrathin and effective carbon nanolayers.

2. Materials and Methods

All the chemicals were of analytic grade and were used without any purification. The $LiMnPO_4$ precursors were prepared with a solvothermal method. In a typical synthesis, H_3PO_4 (80 wt.%, 2.94 g) was mixed with ethylene glycol (EG) (120 mL) in a 250-mL beaker. Then $MnSO_4{\cdot}H_2O$ (5.07 g) was dissolved in water (30 mL) under ultrasonic for 10 min and then added to the H_3PO_4-EG solution mentioned above. Subsequently, $LiOH{\cdot}H_2O$ (3.15 g) was introduced into the mixture solution under stirring to form a light-pink suspension. The mixture was transferred into a 200-mL autoclave after ultrasonic treatment for 30 min. The autoclave was sealed, heated at 150°C for 12 h, and cooled to room temperature. The white product was collected via centrifugation and washed with ethanol and distilled water for 3 times separately. The final product was dried under vacuum at 80°C overnight. For convenience, the obtained pure $LiMnPO_4$ was denoted as LMP. ULMP/C composites were prepared through an EG-assisted pyrolysis method. Firstly, sucrose (0.095 g) was dissolved in the mixture solution of deionized water (1 mL) and EG (0.5 mL) in a 5-mL beaker. The as-prepared LMP precursors (0.50 g) were added into the solution by stirring for ~1 h to form slurry, dried in an oven at 80°C to form solid block, and then heated at 350°C for 1 h and 650°C for 5 h under an Ar flow in a tube furnace. As a reference, $LiMnPO_4$/C composites (named LMP/C) were also prepared through a traditional hydrothermal method according to our reported work [35].

The samples were characterized by X-ray diffraction (XRD, PANalytical X'Pert Pro with Cu K_α radiation, $\lambda = 1.5418$ Å, scanning rate: 2° min^{-1}), thermogravimetric analysis (TG, Perkin Elmer thermobalance, heating rate: 5°C min^{-1}), transmission electron microscopy (TEM, Tecnai G^2F30 S-Twin operated at 300 kV), scanning electron microscopy (SEM), and energy dispersive X-ray spectroscopy (EDS) (Hitachi S-4700 operated at 15 kV).

The electrochemical performances were tested by the assembly of CR2032-type coin cells in an argon-filled glove box (O_2 < 5 ppm and H_2O < 1 ppm). The working electrodes were mixed of active materials, acetylene black (AB), and polyvinylidene fluoride (PVDF) with a weight ratio of 70 : 20 : 10. N-Methylpyrrolidone (NMP) was used as the solvent. The average weight of the working electrodes was approximately 0.8 mg. Lithium metal was used as the counter and reference electrode. Al and Cu foils were adopted as the current collectors for the cathode and anode, respectively. Celgard 2400 was used as the separator. The electrolyte was 1 M $LiPF_6$ dissolved in a 1 : 1 : 1 volume ratio of ethylene carbonate (EC), ethylene methyl carbonate (EMC), and dimethyl carbonate (DMC). Cycling measurements were carried out at the voltage range of 2.0–4.5 V under a Land-CT2001A instrument at 25°C. Cyclic voltammetry (CV) was performed with a CHI660B. All the tested capacities were based on the whole weight of samples.

3. Results and Discussion

The synthesis process and formation mechanism of the ultrathin carbon layer by the EG-assisted method can be schematically illustrated in Scheme 1. Note that, ethylene glycol (EG) played an essential and unique role in this process. Firstly, EG was a good dispersant for water and sucrose. Both the EG and sucrose had abundant -OH groups, which made it easy to form EG-sucrose complexes especially during heating. More importantly, the C-O of EG possessed a pair of electrons and its ability to be a donor of oxygen atoms that enabled it to couple with Mn^{2+} ions on the surface of $LiMnPO_4$ [36]. When mixing with $LiMnPO_4$ particles, EG-sucrose complexes can tightly and uniformly encapsulate the particles and convert into ultrathin carbon layer after calcination at high temperatures.

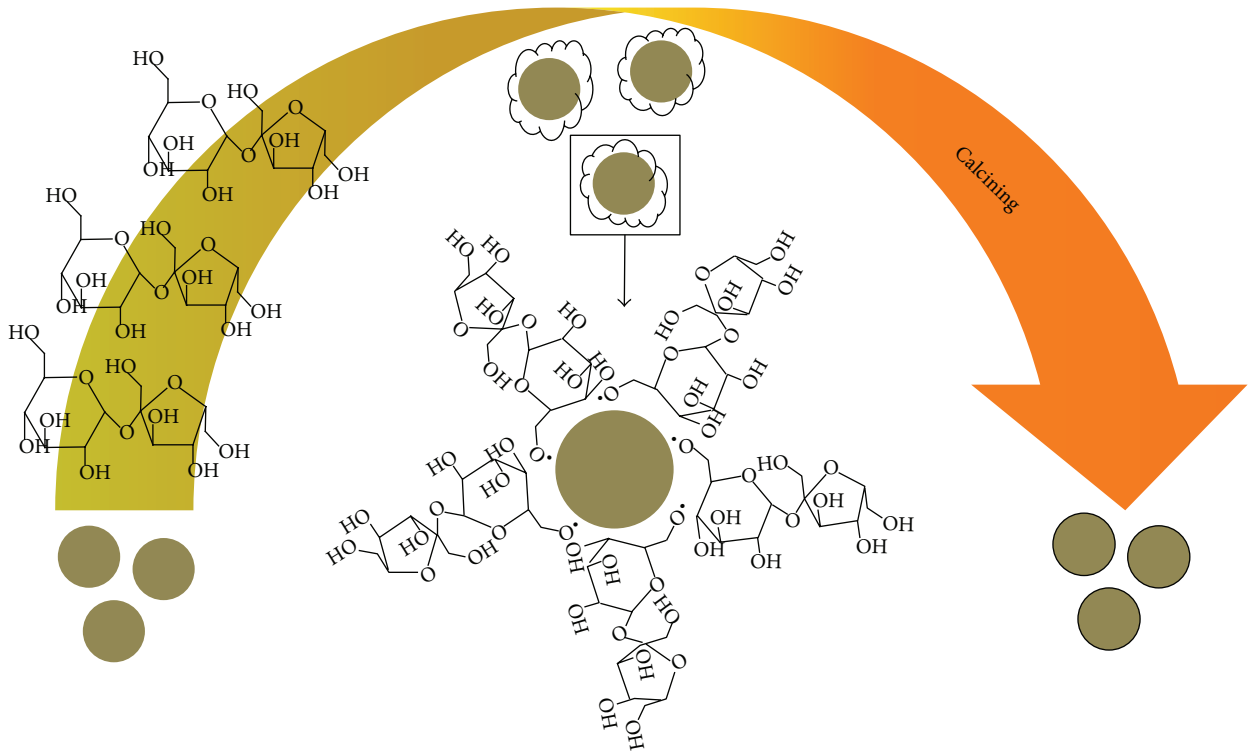

Scheme 1: Schematic illustration of the EG-assisted method for ULMP/C composites.

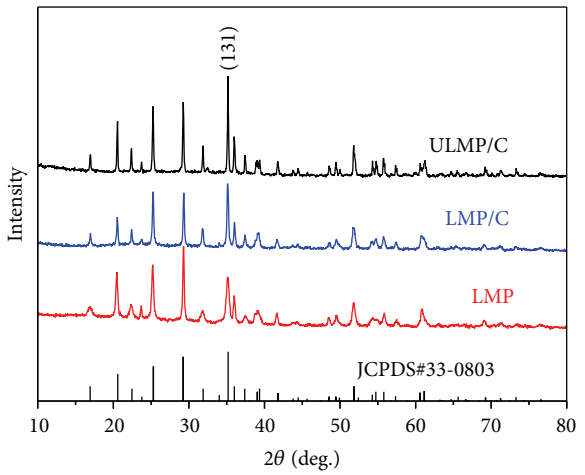

Figure 1: XRD patterns of pure LMP, LMP/C, and ULMP/C composites.

Figure 1 shows XRD patterns of pure LMP, LMP/C, and ULMP/C composites. All the diffraction peaks of pure LMP were clearly indexed to the standard card of orthorhombic $LiMnPO_4$ (JCPDS 33-0804, space group: *Pmnb*, $a = 6.106$ Å, $b = 10.454$ Å, $c = 4.749$ Å). The strong peaks at 20.5°, 25.3°, 29.2°, and 35.1° can be assigned to the (0 1 1), (1 1 1), (2 0 0), and (1 3 1) plane of $LiMnPO_4$, respectively. Interestingly, LMP/C and ULMP/C presented a different (1 3 1) peak at 35.1° with much stronger intensity. All the peaks were in good agreement with the standard card of orthorhombic $LiMnPO_4$ (JCPDS 33-0803, space group: *Pmnb*, $a = 6.108$ Å, $b = 10.459$ Å, $c = 4.732$ Å). The conversion of crystal form mainly came from the high-temperature annealing. No obvious other peaks were detected for impurities.

SEM, TEM, and EDS were performed to confirm the morphology, structure, and element distribution of LMP/C and ULMP/C composites (Figure 2). Figures 2(a) and 2(b) show that LMP/C composites derived from the traditional hydrothermal treatment consisted of nanoparticles (50–100 nm in length or thickness) with irregular shapes. In general, it was difficult for the hydrothermal method to realize the perfect carbon coating on $LiMnPO_4$ without any surface

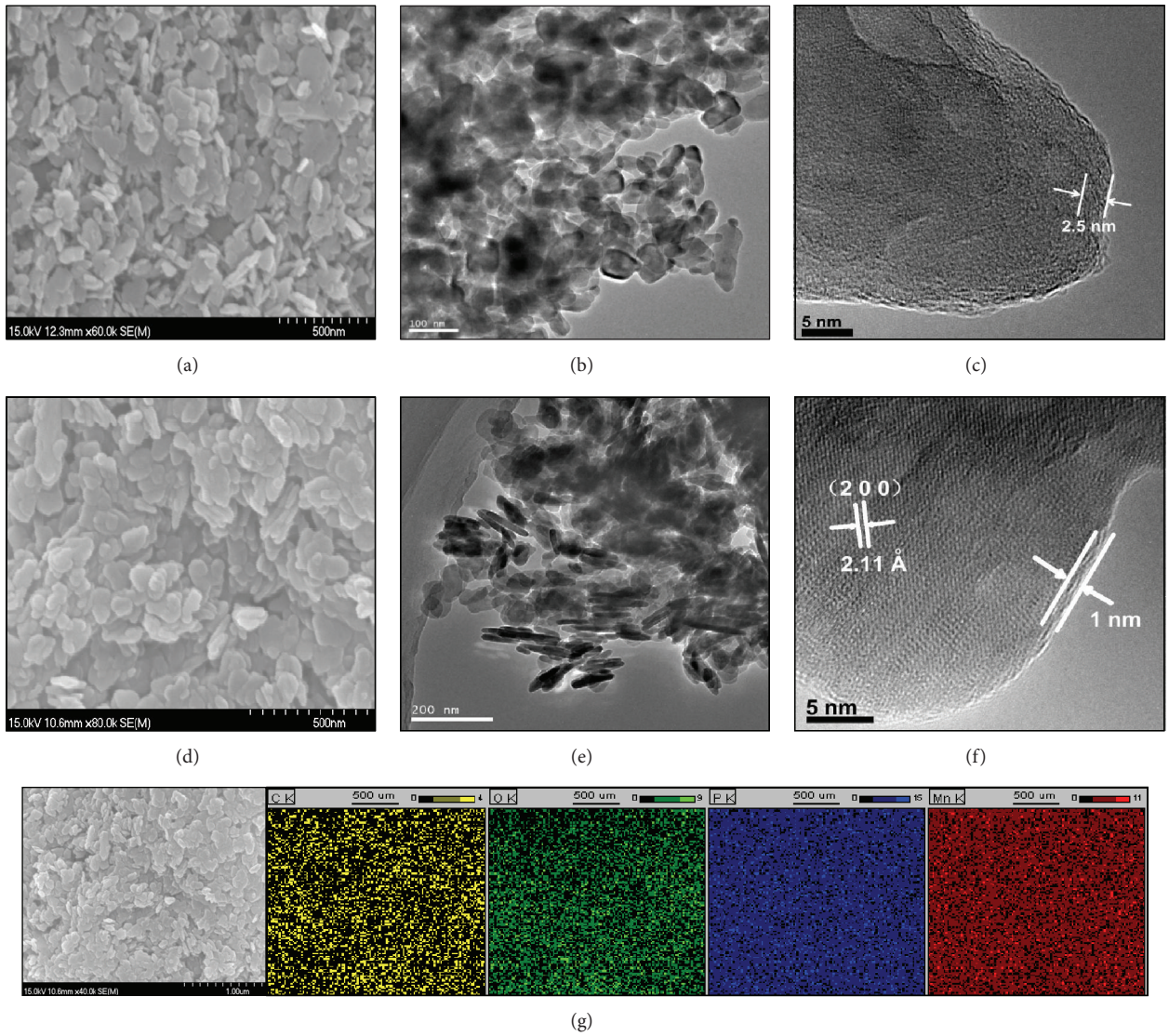

Figure 2: (a) SEM and (b, c) TEM images of LMP/C; (d) SEM and (e, f) TEM images of ULMP/C; (g) EDS mapping results of ULMP/C.

modification. As shown in Figure 2(c), the carbon layer was incomplete and nonuniform although the carbon content reached 13 wt.% (see TG analysis below). In fact, carbon microspheres also formed during the hydrothermal process. Another negative effect of the hydrothermal treatment was that $LiMnPO_4$ precursors had another crystalline reformation and grew up into bigger particles to some extent (Figure 2(b)).

In comparison, the EG-assisted pyrolysis method provided an ultrathin and well-proportioned coating nanolayer with a very limited carbon and simultaneously maintained the morphology of precursors to the greatest extent. Figure 2(d) shows that ULMP/C particles had similar morphology and particle sizes with LMP/C. However, Figure 2(e) demonstrates that the composites mainly consisted of nanoplates (less than 50 nm in thickness). HRTEM can clearly confirm that an amorphous and ultrathin carbon layer (~1 nm in thickness) was uniformly coated on the crystalline particles (Figure 2(f)). The lattice distance of 3.11 Å was well assigned to the (2 0 0) plane of orthorhombic $LiMnPO_4$ (JCPDS 33-0803). The EDS mapping (Figure 2(g)) can further illustrate the uniform distribution of all the elements of Mn, P, O, and C in ULMP/C composites. Profiting from these favorable features, ULMP/C nanoplates exhibited a preferable performance than pure LMP and LMP/C.

The carbon contents in ULMP/C and LMP/C composites can be confirmed by TG curves (Figure 3). The small amount of mass loss (~1 wt.%) before 300°C can be ascribed to the removing of the water absorbed on the particle surface. The rapid weight loss from 300°C came from the dramatic oxidation of carbon, since $LiMnPO_4$ was stable in air at 20–700°C. Therefore, the carbon contents in ULMP/C and LMP/C composites should be ~2 wt.% and 13 wt.%, respectively. The carbon layer greatly improved the electron conductivity of $LiMnPO_4$. In addition, it can effectively prevent the direct contact between the active material and electrolyte and

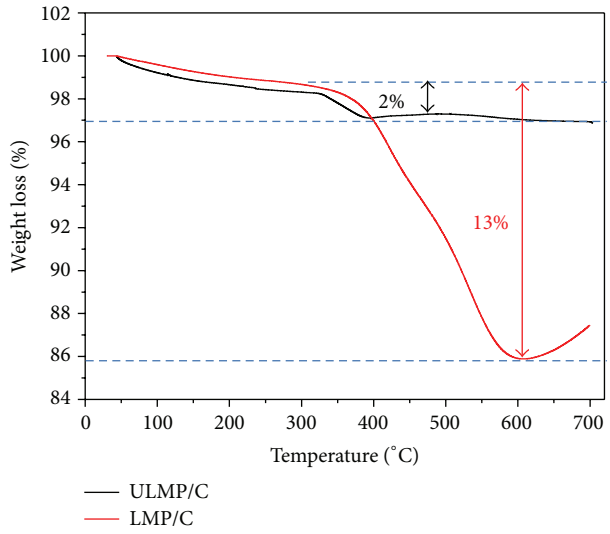

Figure 3: TG curves of ULMP/C and LMP/C composites at 20–700°C in air.

postpone the attack from HF acid and the dissolution of Mn [37].

Profiting from the small $LiMnPO_4$ particle size and especially the ultrathin and uniform carbon nanolayer, ULMP/C nanoplates demonstrated a considerable lithium storage capacity and rate performances. Figure 4 showed the charge/discharge profiles of LMP, LMP/C, LMP/C without EG, and ULMP/C at a current density of 0.1 C (1 C = 170 mA g^{-1}). As shown in Figure 4(a), pure LMP was almost inert for lithium storage and exhibited very poor capacities (only 16 mAh g^{-1} for the 1st charge). In comparison, with the help of carbon coating, LMP/C and ULMP/C composites displayed much better voltage plateaus and higher capacities (~160 mAh g^{-1} for the first charge) (Figures 4(b) and 4(d)). The initial Coulombic efficiency of ULMP/C was 88.3%, much higher than that (54.8%) of LMP/C. The flat plateaus at ~4.1/4.2 V should be ascribed to the insertion/extraction of Li^+ ions from $LiMnPO_4$. The reduced polarization came from the increased electronic conductivity owing to the ultrathin carbon layer. Figure 4(c) exhibited the poor capacity of LMP/C without EG. The initial charge and discharge capacities were 79 and 67 mAh g^{-1}, respectively. However, the reversible capacities rapidly reduced to ~20 mAh g^{-1}, much lower than the counterpart of ULMP/C composites. The obvious difference came from the ununiformed carbon of $LiMnPO_4$/C particles without EG. Figure 4(e) presents the CV curves of ULMP/C for the initial 3 cycles at a scanning rate of 0.1 mV s^{-1}. The oxidation peak at ~4.3 V corresponded to the extraction of Li^+ ions from $LiMnPO_4$, while the reduction peak at ~3.9 V was assigned to the reversible insertion of Li^+ ions, which is in good agreement with the voltage plateaus of charge-discharge profiles. The oxidation and reduction peaks seem to be symmetric, indicating a good reversibility. The almost overlapped curves for the 2nd and 3rd cycles suggested the improved kinetics and better cycling stability. The EIS spectra were performed to investigate the charge transport kinetics for the electrochemical behaviors of the samples (Figure 4(f)). It is clear that the semicircles in the high-to-medium frequency range for ULMP/C was much smaller than that of pure LMP and LMP/C, indicating that the ultrathin carbon coating on the surface of $LiMnPO_4$ could greatly improve the charge transfer ability of Li^+ ions at the interface between the electrolyte. The charge transfer should be much easier for the ultrathin carbon layer in ULMP/C.

As shown in Figure 5(a), the reversible capacity of pure LMP was only ~2 mAh g^{-1} after 50 cycles. Benefiting from the enhanced conductivity, LMP/C exhibited an initial reversible capacity of 96.5 mAh g^{-1} which reduced to 68 mAh g^{-1} (~70% retention) after 50 cycles, while the initial reversible capacity of ULMP/C reached 130.8 mAh g^{-1} and maintained 108.5 mAh g^{-1} (~83% retention) after 50 cycles. The ULMP/C composites also demonstrated much better rate performances than pure LMP and LMP/C (Figure 5(b)). When the current densities increased stepwise from 0.05 C to 0.1 C, 0.2 C, 0.3 C, and 0.5 C, the reversible capacities were approximately 130, 115, 100, 90, and 80 mAh g^{-1}, respectively. When the rate returned to 0.05 C again, an average capacity of 120 mAh g^{-1} could be recovered. All these values were much higher than the counterpart of pure LMP and LMP/C composites.

The obviously enhanced performance of ULMP/C can be attributed to the ultrathin and well-proportioned carbon coating layer. (i) In comparison with pure LMP, ULMP/C possessed better electronic conductivity due to the existence of carbon network. (ii) Profiting from the ultrasmall content (2 wt.%) of carbon, ULMP/C had much more active components (98 wt.%) for lithium storage. In comparison, the $LiMnPO_4$ content in LMP/C was only ~87 wt.%. (iii) Although the carbon in the ULMP/C was very limited, the well-proportioned encapsulation made it more effective than the 13 wt.% carbon in LMP/C to avoid the dissolution/loss of Mn and hence maintained a good support integrity and cycling stability.

4. Conclusions

In summary, ULMP/C nanocomposites, consisting of small $LiMnPO_4$ nanoplates and preferable carbon coating (~1 nm in thickness, 2 wt.%), were prepared through an EG-assisted pyrolysis method. The obtained ULMP/C nanoplates demonstrated much higher reversible capacities (110.9 mAh g^{-1} after 50 cycles at 0.1 C) and rate performances than that of pure LMP and LMP/C composites from the hydrothermal carbon coating route. The enhanced performance can be mainly attributed to the ultrathin and well-proportioned carbon coating nanolayer, which not only significantly improved the conductivity of $LiMnPO_4$ but also effectively protected the active particles from the attack from HF acid and the dissolution of Mn^{2+} ions. This facile and efficient EG-assisted method can enlighten us on exploiting advanced routes to

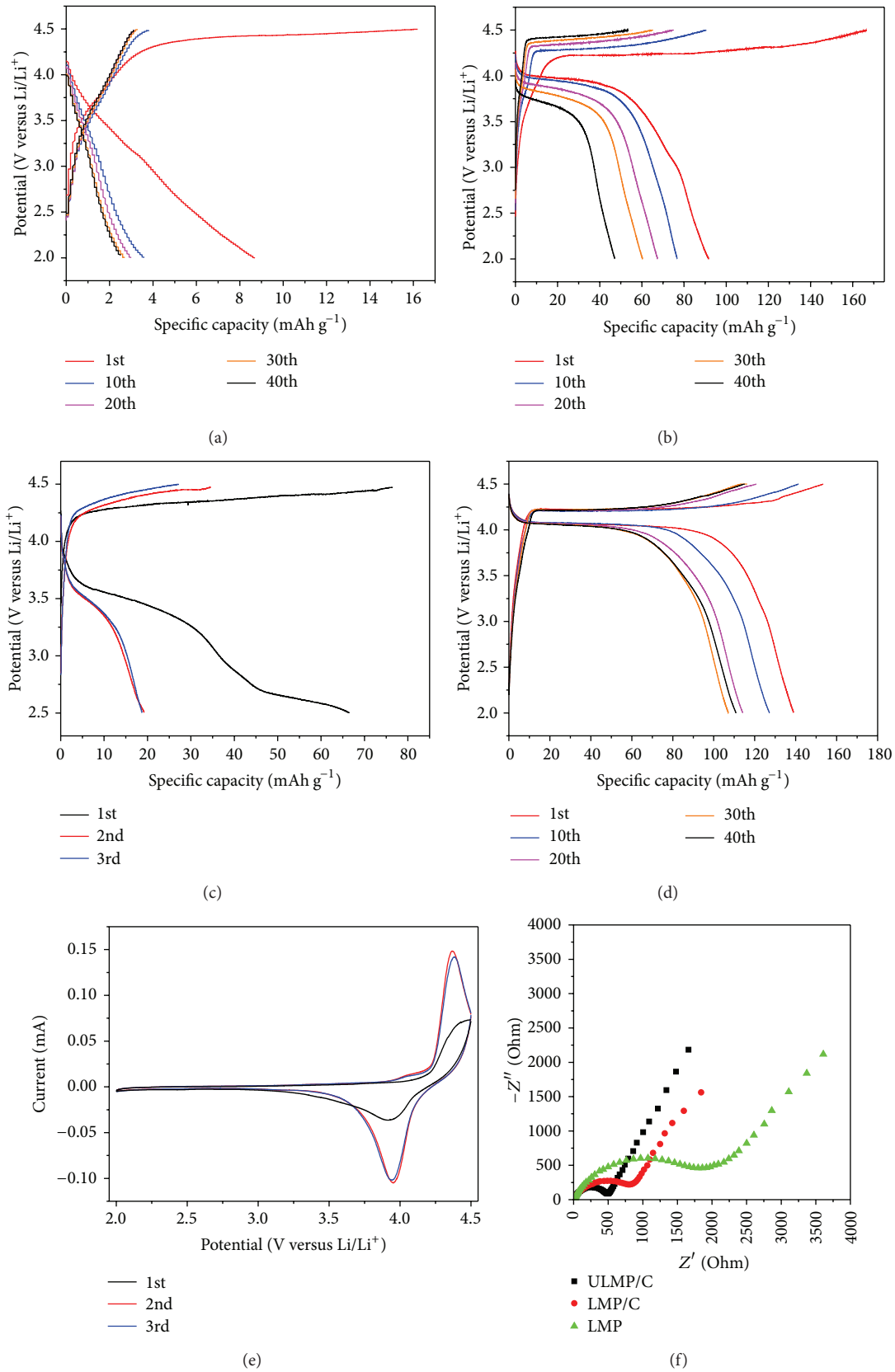

Figure 4: The charge-discharge curves of (a) LMP, (b) LMP/C, (c) LMP/C without EG, and (d) ULMP/C at 0.1 C. (e) CV curves of ULMP/C at a scanning rate of 0.1 mV s^{-1}. (f) Nyquist plots of LMP, LMP/C, and ULMP/C after 5 cycles.

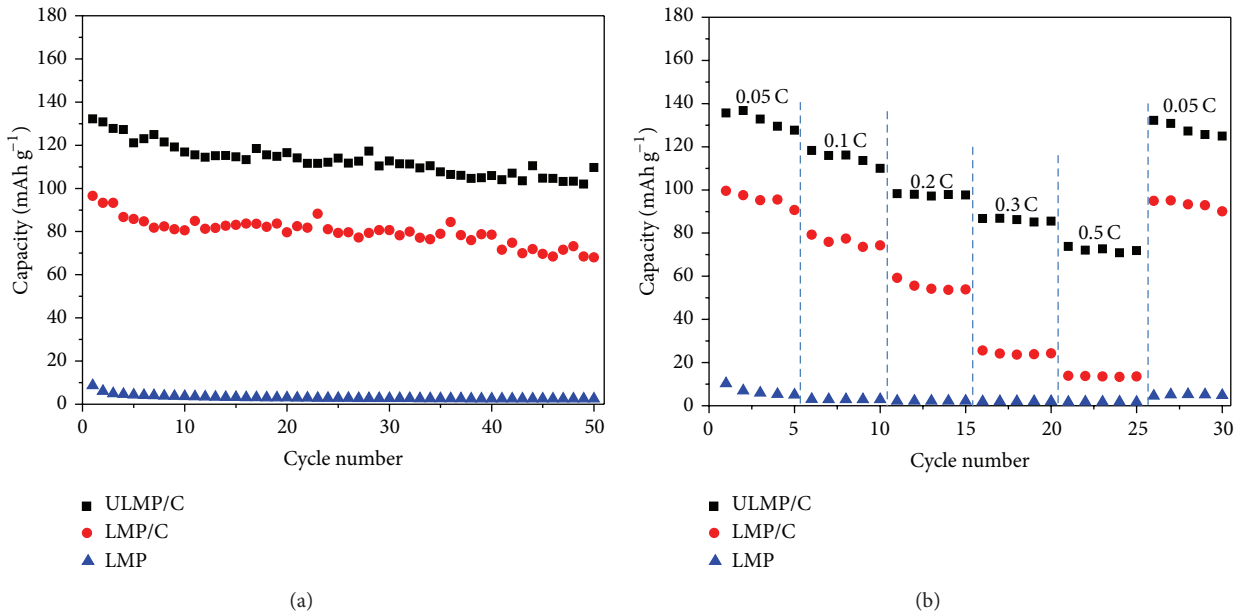

Figure 5: (a) Long-term cycling performance (at 0.1 C) and (b) rate performance of LMP, LMP/C, and ULMP/C.

modify active materials with ultrathin and homogeneous carbon layers.

Conflict of Interests

The authors declare that there is no conflict of interests regarding the publication of this paper.

Acknowledgments

This work was supported by the International Science and Technology Cooperation Program of China (2012CI4027) and the National Natural Science Foundation of China (21403195).

References

[1] M. Armand and J. M. Tarascon, "Building better batteries," *Nature*, vol. 451, no. 7179, pp. 652–657, 2008.

[2] P. G. Bruce, B. Scrosati, and J.-M. Tarascon, "Nanomaterials for rechargeable lithium batteries," *Angewandte Chemie—International Edition*, vol. 47, no. 16, pp. 2930–2946, 2008.

[3] M. S. Whittingham, "Lithium batteries and cathode materials," *Chemical Reviews*, vol. 104, no. 10, pp. 4271–4301, 2004.

[4] B. Sadeghi, R. Sarraf-Mamoory, and H. R. Shahverdi, "Surface modification of $LiMn_2O_4$ for lithium batteries by nanostructured $LiFePO_4$ phosphate," *Journal of Nanomaterials*, vol. 2012, Article ID 743236, 7 pages, 2012.

[5] L. Chen, M. Zhang, and W. Wei, "Graphene-based composites as cathode materials for lithium ion batteries," *Journal of Nanomaterials*, vol. 2013, Article ID 940389, 8 pages, 2013.

[6] S. L. Shang, Y. Wang, Z. G. Mei, X. D. Hui, and Z. K. Liu, "Lattice dynamics, thermodynamics, and bonding strength of lithium-ion battery materials $LiMPO_4$ (M = Mn, Fe, Co, and Ni): a comparative first-principles study," *Journal of Materials Chemistry*, vol. 22, no. 3, pp. 1142–1149, 2012.

[7] X. Sun, C. Yan, Y. Chen et al., "Three-dimensionally 'curved' NiO nanomembranes as ultrahigh rate capability anodes for Li-ion batteries with long cycle lifetimes," *Advanced Energy Materials*, vol. 4, no. 4, 2014.

[8] M. M. Ren, Z. Zhou, L. W. Su, and X. P. Gao, "$LiVOPO_4$: a cathode material for 4V lithium ion batteries," *Journal of Power Sources*, vol. 189, no. 1, pp. 786–789, 2009.

[9] L. Su, Y. Jing, and Z. Zhou, "Li ion battery materials with core-shell nanostructures," *Nanoscale*, vol. 3, no. 10, pp. 3967–3983, 2011.

[10] H. Li, Y. Wang, X. Yang, L. Liu, L. Chen, and J. Wei, "Improved electrochemical performance of 5 V $LiCoPO_4$ cathode materials via yttrium doping," *Solid State Ionics*, vol. 255, pp. 84–88, 2014.

[11] M. Zhen, L. Su, Z. Yuan, L. Liu, and Z. Zhou, "Well-distributed TiO_2 nanocrystals on reduced graphene oxides as high-performance anode materials for lithium ion batteries," *RSC Advances*, vol. 3, no. 33, pp. 13696–13701, 2013.

[12] L. Dimesso, C. Förster, W. Jaegermann et al., "Developments in nanostructured $LiMPO_4$ (M = Fe, Co, Ni, Mn) composites based on three dimensional carbon architecture," *Chemical Society Reviews*, vol. 41, no. 15, pp. 5068–5080, 2012.

[13] X. Chen, C. Li, M. Grätzel, R. Kostecki, and S. S. Mao, "Nanomaterials for renewable energy production and storage," *Chemical Society Reviews*, vol. 41, no. 23, pp. 7909–7937, 2012.

[14] N. N. Bramnik and H. Ehrenberg, "Precursor-based synthesis and electrochemical performance of $LiMnPO_4$," *Journal of Alloys and Compounds*, vol. 464, no. 1-2, pp. 259–264, 2008.

[15] G. Li, H. Azuma, and M. Tohda, "$LiMnPO_4$ as the cathode for lithium batteries," *Electrochemical and Solid-State Letters*, vol. 5, no. 6, pp. A135–A137, 2002.

[16] M. Minakshi, P. Singh, S. Thurgate, and K. Prince, "Electrochemical behavior of olivine-type $LiMnPO_4$ in aqueous solutions," *Electrochemical and Solid-State Letters*, vol. 9, no. 10, pp. A471–A474, 2006.

[17] T. Shiratsuchi, S. Okada, T. Doi, and J.-I. Yamaki, "Cathodic performance of $LiMn_{1-x}M_xPO_4$ (M = Ti, Mg and Zr) annealed in an inert atmosphere," *Electrochimica Acta*, vol. 54, no. 11, pp. 3145–3151, 2009.

[18] H. Li, Y. Li, L. Chen et al., "Microwave assisted synthesis of core–shell $LiFe_{1/3}Mn_{1/3}Co_{1/3}PO_4$/C nanocomposite cathode for high-performance lithium-ion batteries," *Journal of Alloys and Compounds*, vol. 617, pp. 154–159, 2014.

[19] R. Dominko, M. Bele, M. Gaberscek et al., "Porous olivine composites synthesized by sol-gel technique," *Journal of Power Sources*, vol. 153, no. 2, pp. 274–280, 2006.

[20] G. Chen, J. D. Wilcox, and T. J. Richardson, "Improving the performance of lithium manganese phosphate through divalent cation substitution," *Electrochemical and Solid-State Letters*, vol. 11, no. 11, pp. A190–A194, 2008.

[21] D. Rangappa, K. Sone, Y. Zhou, T. Kudo, and I. Honma, "Size and shape controlled $LiMnPO_4$ nanocrystals by a supercritical ethanol process and their electrochemical properties," *Journal of Materials Chemistry*, vol. 21, no. 39, pp. 15813–15818, 2011.

[22] C. Delacourt, P. Poizot, M. Morcrette, J.-M. Tarascon, and C. Masquelier, "One-Step low-temperature route for the preparation of electrochemically active $LiMnPO_4$ powders," *Chemistry of Materials*, vol. 16, no. 1, pp. 93–99, 2004.

[23] X. Sun, W. Si, L. Xi et al., "In situ-formed, amorphous, oxygen-enabled germanium anode with robust cycle life for reversible lithium storage," *ChemElectroChem*, 2015.

[24] C. Delacourt, P. Poizot, S. Levasseur, and C. Masquelier, "Size effects on carbon-free $LiFePO_4$ powders: the key to superior energy density," *Electrochemical and Solid-State Letters*, vol. 9, no. 7, pp. A352–A355, 2006.

[25] D. H. Kim and J. Kim, "Synthesis of $LiFePO_4$ nanoparticles in polyol medium and their electrochemical properties," *Electrochemical and Solid-State Letters*, vol. 9, no. 9, pp. A439–A442, 2006.

[26] T. Drezen, N.-H. Kwon, P. Bowen, I. Teerlinck, M. Isono, and I. Exnar, "Effect of particle size on $LiMnPO_4$ cathodes," *Journal of Power Sources*, vol. 174, no. 2, pp. 949–953, 2007.

[27] T. N. L. Doan and I. Taniguchi, "Cathode performance of $LiMnPO_4$/C nanocomposites prepared by a combination of spray pyrolysis and wet ball-milling followed by heat treatment," *Journal of Power Sources*, vol. 196, no. 3, pp. 1399–1408, 2011.

[28] F. Wang, J. Yang, P. Gao, Y. Nuli, and J. Wang, "Morphology regulation and carbon coating of $LiMnPO_4$ cathode material for enhanced electrochemical performance," *Journal of Power Sources*, vol. 196, no. 23, pp. 10258–10262, 2011.

[29] N. P. W. Pieczonka, Z. Liu, A. Huq, and J.-H. Kim, "Comparative study of $LiMnPO_4$/C cathodes synthesized by polyol and solid-state reaction methods for Li-ion batteries," *Journal of Power Sources*, vol. 230, pp. 122–129, 2013.

[30] S. K. Martha, B. Markovsky, J. Grinblat et al., "$LiMnPO_4$ as an advanced cathode material for rechargeable lithium batteries," *Journal of the Electrochemical Society*, vol. 156, no. 7, pp. A541–A552, 2009.

[31] X. Sun, W. Si, X. Liu et al., "Multifunctional Ni/NiO hybrid nanomembranes as anode materials for high-rate Li-ion batteries," *Nano Energy*, vol. 9, pp. 168–175, 2014.

[32] Z. Bakenov and I. Taniguchi, "Physical and electrochemical properties of $LiMnPO_4$/C composite cathode prepared with different conductive carbons," *Journal of Power Sources*, vol. 195, no. 21, pp. 7445–7451, 2010.

[33] Z. Bakenov and I. Taniguchi, "Electrochemical performance of nanocomposite $LiMnPO_4$/C cathode materials for lithium batteries," *Electrochemistry Communications*, vol. 12, no. 1, pp. 75–78, 2010.

[34] S. M. Yuan, J. X. Li, L. T. Yang, L. W. Su, L. Liu, and Z. Zhou, "Preparation and lithium storage performances of mesoporous Fe_3O_4@C microcapsules," *ACS Applied Materials and Interfaces*, vol. 3, no. 3, pp. 705–709, 2011.

[35] L. Su, Y. Zhong, J. Wei, and Z. Zhou, "Preparation and electrochemical Li storage performance of MnO@C nanorods consisting of ultra small MnO nanocrystals," *RSC Advances*, vol. 3, no. 23, pp. 9035–9041, 2013.

[36] J. A. Crisp, R. M. Meier, J. S. Overby, T. P. Hanusa, A. L. Rheingold, and W. W. Brennessel, "Indenyl complexes of manganese(II). Conformational flexibility of the manganese(II)–($R_nC_9H_{7-n}$) bond," *Organometallics*, vol. 29, no. 10, pp. 2322–2331, 2010.

[37] H. Li, Y. Chen, L. Chen et al., "Improved cycling and high rate performance of core-shell $LiFe_{1/3}Mn_{1/3}Co_{1/3}PO_4$/carbon nanocomposites for lithium-ion batteries: effect of the carbon source," *Electrochimica Acta*, vol. 143, pp. 407–414, 2014.